Analyst

PAPER

View Article Online
View Journal | View Issue

Cite this: *Analyst*, 2015, **140**, 6005

Reconstructing accurate ToF-SIMS depth profiles for organic materials with differential sputter rates†

Adam J. Taylor,[a,b] Daniel J. Graham[a,c] and David G. Castner*[a,b,c]

To properly process and reconstruct 3D ToF-SIMS data from systems such as multi-component polymers, drug delivery scaffolds, cells and tissues, it is important to understand the sputtering behavior of the sample. Modern cluster sources enable efficient and stable sputtering of many organics materials. However, not all materials sputter at the same rate and few studies have explored how different sputter rates may distort reconstructed depth profiles of multicomponent materials. In this study spun-cast bilayer polymer films of polystyrene and PMMA are used as model systems to optimize methods for the reconstruction of depth profiles in systems exhibiting different sputter rates between components. Transforming the bilayer depth profile from sputter time to depth using a single sputter rate fails to account for sputter rate variations during the profile. This leads to inaccurate apparent layer thicknesses and interfacial positions, as well as the appearance of continued sputtering into the substrate. Applying measured single component sputter rates to the bilayer films with a step change in sputter rate at the interfaces yields more accurate film thickness and interface positions. The transformation can be further improved by applying a linear sputter rate transition across the interface, thus modeling the sputter rate changes seen in polymer blends. This more closely reflects the expected sputtering behavior. This study highlights the need for both accurate evaluation of component sputter rates and the careful conversion of sputter time to depth, if accurate 3D reconstructions of complex multi-component organic and biological samples are to be achieved. The effects of errors in sputter rate determination are also explored.

Received 30th April 2015,
Accepted 9th July 2015

DOI: 10.1039/c5an00860c

www.rsc.org/analyst

Introduction

The capability of argon gas cluster ion beam (GCIB) sources to effectively sputter organic materials with minimal surface damage has expanded the range of systems that may be studied by ToF-SIMS sputter depth profiling and 3D imaging. These include multicomponent organic systems that form key components of diverse technologies including organic photovoltaics[1] drug eluting stents[2,3] and model polymeric multilayer systems.[4,5] Argon cluster sources have proved similarly valuable for the analysis of biological materials such as amino acids,[6] lipids[7] and peptides.[8] Analysis by ToF-SIMS has the potential to provide useful information about the composition, dimensions and spatial locations of features, interfaces and defects in such systems. However, answering questions about these systems requires accurate calibration and scaling along the *z*-axis (depth) during analysis of depth profiles and 3D images. When a uniform sputter rate through the sample, including the substrate, may be assumed, depth profile calibration can be performed by simply calculating a single sputter rate based on the time to sputter to the location of a known feature. The location of other features and interfaces can then be inferred directly from the sputter time required to reach the area of interest. However, many organic materials sputter at different rates.[9,10] Such differences in sputtering may introduce a number of artifacts, which require careful consideration during data reconstruction. These include the distortion of apparent feature dimensions and spatial locations. These artifacts become more pronounced as the difference in sputter rates increases.

The analysis and reconstruction of depth profiles has been of interest to researchers using both XPS and SIMS. Of particular interest is the ability to determine interface and delta layer positions within multilayer or mixed systems.[11–14] Several studies have described the need for, and methods of, correcting for a number of depth profiling artifacts. These include

[a]*National ESCA and Surface Analysis Center for Biomedical Problems (NESAC/BIO), Molecular Engineering and Sciences Institute, University of Washington, Seattle, WA, USA. E-mail: castner@uw.edu; Tel: +1 206-543-8094*
[b]*Department of Chemical Engineering, University of Washington, Seattle, WA, USA*
[c]*Department of Bioengineering, University of Washington, Seattle, WA, USA*
† Electronic supplementary information (ESI) available. See DOI: 10.1039/c5an00860c

changing sputter rates in highly topographic samples,[15] and beam-damage induced sputter rate deterioration.[16,17] However, few studies have used methods to identify and correct for different component sputter rates.[18,19] In some cases differences in sputter rates may be minimized through careful selection of cluster size and energy.[9] However, this may not provide sufficient range of sputter-rate manipulation. Approaches to dynamically measure sputter yield, through a quartz crystal microbalance[10] or secondary neutral mass spectrometry,[20] have been proposed. More simply, correction for different sputter rates can be applied during depth calibration using component sputter rates calculated from single-component films. This study demonstrates the application and value of such *post-hoc* correction in a spun-cast polystyrene–PMMA bilayer system. This polymer pairing was selected due to its previously demonstrated differences in sputter rate.[9]

In this study we demonstrate that (1) when differences in sputter rates between components are not taken into account reconstructed depth profiles are inaccurate; (2) application of individual component sputter rates allows for accurate depth profiles to be transformed from sputter time/dose to depth; (3) accounting for the transition between different sputter rates across an interface may further improve profile reconstruction; and (4) that small deviations in sputter rate determination can have significant effects on the reconstructed depth profile.

Results and discussion

Characterization of single-component and bilayer films

Thin polymer films of polystyrene and PMMA, and bilayers of polystyrene on PMMA, were prepared by spin-casting from selective solvents. XPS analysis of single-component and bilayer films was performed to validate composition of single component films and assess continuity of the polystyrene overlayer in bilayer films. XPS spectra and calculated atomic percentages for both polystyrene and PMMA are in agreement with those previously reported for these materials.[21–24] Table 1A shows atomic percentages of carbon and oxygen derived from XPS survey spectra. Atomic percentages of carbon and oxygen in single component films are in agreement with the expected stoichiometry. Fig. 1 shows XPS high resolution C1s scans from representative PMMA, polystyrene, and bilayer films. In the C1s region, polystyrene exhibits a single peak at 285 eV, representing the C–H bond and a small peak near 292 eV representing the π–π* shakeup characteristic of the π bonds in the aromatic ring. PMMA exhibits a more complex C1s peak with peaks at 285 eV (C–C/C–H), 286.6 eV (C–O–C) and 288.8 eV (O–C═O). These regions are quantified in Table 1B. The C1s region for the bilayer sample appears identical to those for pure polystyrene, with a single peak at 285 eV and a π–π* shakeup peak near 292 eV. Additionally the atom percentage of oxygen in the bilayer films is <1%. This suggests that the polystyrene forms an intact overlayer, providing complete coverage of the underlying PMMA. This is in line with previous reports detailing selection of 1-chloropentane as an optimal solvent for directly spin casting polystyrene overlayers on PMMA.[25]

Table 1 (A) Atomic percentages of carbon and oxygen derived from C1s and O1s regions in XPS survey spectra. (B) Area percentages for C–C, C–O–C and O–C═O components of the C1s region for PMMA, polystyrene and bilayer spun-cast polymer films. Values represent mean ± 1 standard deviation, n = 3. NR represents no measured peak for that component

	Atom percentages from survey scan		
A	PMMA	Polystyrene	Bilayer
Carbon	72.0 ± 0.8	99.1 ± 1.0	99.9 ± 0.7
Oxygen	28.0 ± 0.8	0.9 ± 1.0	0.1 ± 0.7
	Area percentages from C1s components		
B	PMMA	Polystyrene	Bilayer
C–C	54.9 ± 0.1	94.7 ± 0.6	94.7 ± 0.6
C–O	26.7 ± 0.4	NR	NR
C═O	18.4 ± 0.5	NR	NR
π–π*	NR	5.3 ± 0.6	5.3 ± 0.6

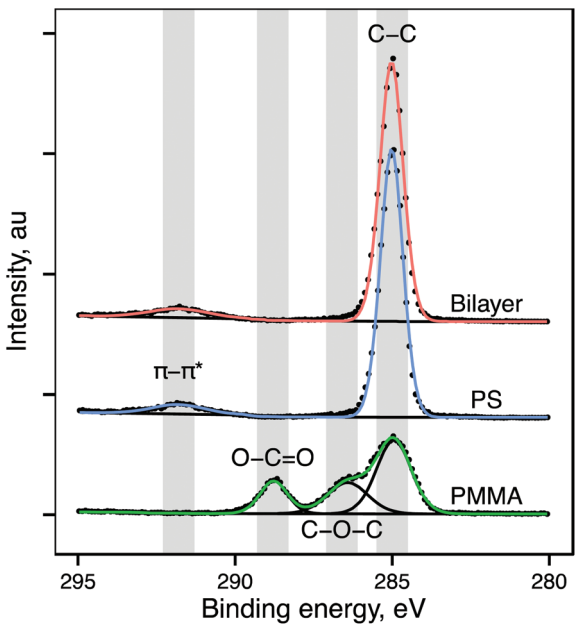

Fig. 1 Representative high-resolution XPS scans of the C1s region for PMMA (bottom), polystyrene (center) and bilayer (top) spun-cast polymer films on Si wafer. Presence of the π–π* shakeup peak and absence of C–O–C and O–C═O peaks (fitted components shown in black) in bilayer sample suggests the presence of an intact polystyrene overlayer atop initially deposited PMMA film.

Determination of sputter rates

To define an accurate sputter rate, the sputter time or dose through a known thickness of material is required. Table 2 shows measured film thicknesses and sputter times to the

Table 2 Measured thicknesses and sputter times through PMMA and polystyrene films and calculated sputter rates and sputter yields. Thickness determined by AFM measurement of trench cut in film. Sputter time to Si interface determined by position of maxima of first derivative. Values represent mean ± 1 standard deviation. n = 3 for both sputter time and thickness measurements, except for representative bilayer where n = 2. Sputter rate calculated as thickness/time to interface

Film type	Thickness, nm	Sputter time to Si interface, s	Sputter rate, nm s^{-1}	Sputter yield, nm^3 per atom
PMMA	105 ± 5	22.4 ± 0.2	4.69 ± 0.24	0.108 ± 0.006
Polystyrene	114 ± 7	48.3 ± 1.6	2.37 ± 0.16	0.055 ± 0.004
Bilayer	223 ± 9	69.0 ± 0.1	3.23 ± 0.13	0.075 ± 0.003

polymer–substrate interface, along with the calculated sputter rates, for single component polystyrene and PMMA films. Thicknesses of single component and bilayer films were measured by AFM profiling of a trench cut in the film by a scalpel blade. AFM was chosen as it allows direct measurement of film thickness. Polystyrene single component films have a mean thickness of 114 nm ± 7 nm (mean ± SD) and are slightly thicker than the PMMA single component films, which have a mean thickness of 105 ± 9 nm. Within experimental error, the sum of single component film thicknesses (220 nm) is not significantly different from the measured bilayer film thickness (223 nm), suggesting minimal interfacial mixing prior to depth profiling.

From single-component films we see that PMMA sputters 1.97 times faster than polystyrene with sputter rates of 4.69 nm s^{-1} (PMMA) and 2.37 nm s^{-1} (polystyrene), respectively. These sputter rates may be converted to sputter yields of 0.108 nm^3 per atom (PMMA) and 0.055 nm^3 per atom (polystyrene) respectively, which are closely comparable to literature reported yields for argon clusters of same energy per atom.[26–28] The difference between polystyrene and PMMA sputter rates compares favorably with reported sputter yields for the same polymers, using argon clusters of same energy per atom, in which the sputter yield of PMMA is 2.2 times that of polystyrene.[9] It is important to note that the way in which sputtering rate decreases with sputter ion energy will vary between materials and is a function of variables including primary ion beam type, cluster size and energy.[9,10,27,29]

Depth profile of representative bilayer

Fig. 2A shows a representative ToF-SIMS depth profile through a polystyrene–PMMA bilayer. The intensities of characteristic ions for each layer (polystyrene: $C_7H_7^+$, m/z 91; PMMA: $C_4H_5O^+$, m/z 69; silicon: Si^+, m/z 28) are plotted on a $\log_{10}$ scale against sputter time. Within the initial polystyrene layer the intensity of $C_7H_7^+$ is stable. Between approximately 45 and 55 seconds of sputtering time the intensity of $C_7H_7^+$ falls while that of $C_4H_5O^+$ rises as the profile crosses the polystyrene–PMMA interface. In the underlying PMMA layer the intensity of $C_4H_5O^+$ stabilizes. However, the intensity of $C_7H_7^+$ does not fall to zero, but rather stabilizes at a lower intensity. This is due to the fact that m/z 91.05 is a minor peak in the PMMA spectrum. Additionally a small increase in the intensity of Si^+ is seen at the polystyrene–PMMA interface, likely due to polydimethylsiloxane (PDMS) contamination of the PMMA stock solution. This hypothesis is supported by the appearance of characteristic PDMS peaks including $SiC_3H_9^+$ and $Si_2C_5H_{15}O^+$ in the spectra of PMMA films (data not shown). Beyond 70 seconds of sputter time the polymer–silicon interface is seen as a rapid drop in intensity of $C_4H_5O^+$ and $C_7H_7^+$, corresponding with a significant rise of the Si^+ peak. Beyond ~75 seconds of sputter time the Si^+ intensity stabilizes and the

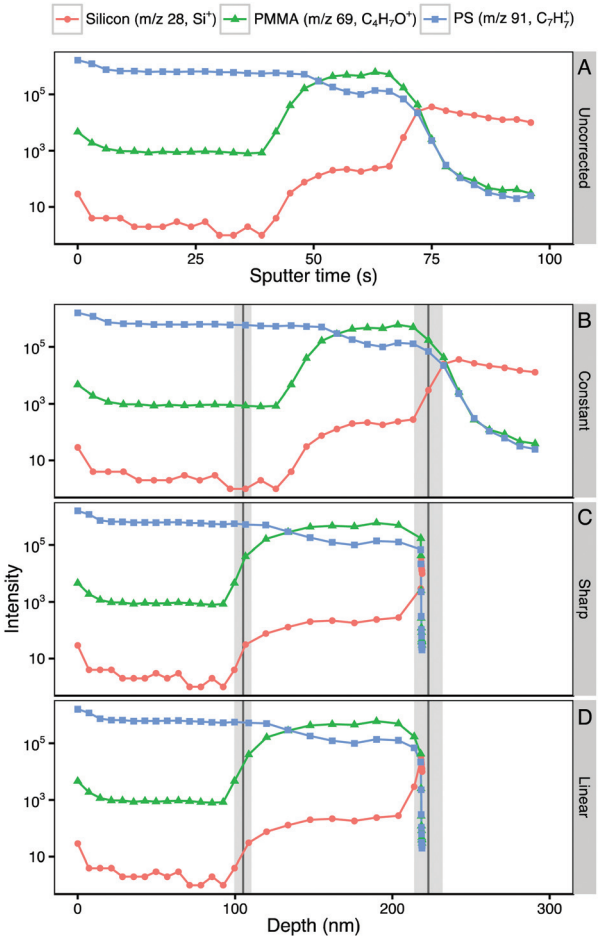

Fig. 2 (A) Representative ToF-SIMS depth profile through a polystyrene–PMMA bilayer spun-cast film on Si wafer plotted against sputter time. (B–D) The same representative ToF-SIMS depth profile transformed to plot depth using different sputter rate assignment methods. (B) Transformation by constant sputter rate defined from measured bilayer thickness and sputter time to polymer–Si interface. (C) Transformation using step change between measured component sputter rates at polystyrene–PMMA and PMMA–Si interfaces. (D) Linear transition between component sputter rates across depth-resolution of polystyrene–PMMA and PMMA–Si interfaces. Intensities of characteristic peaks of each component (silicon: Si^+, m/z 28; PMMA: $C_4H_5O^+$, m/z 69; polystyrene: $C_7H_7^+$, m/z 91) are plotted on a $\log_{10}$ intensity scale against sputter time (a) or depth from surface (b–d). Expected position of polystyrene–PMMA and PMMA–Si interfaces from AFM measurements of single-component and bilayer films are shown as vertical line (mean) and shaded area (±1 SD).

intensities of characteristic polymer peaks continue to fall in intensity. Throughout the depth profiles, no pinholes or defects were observed in ion images (data not shown), suggesting that films are intact and laterally homogeneous.

In many cases it is sufficient to interpret depth profiles when plotted on their original axis of sputter time or ion dose. These include systems where components sputter at similar rates and where interfaces positions are tightly controlled by processing variables or otherwise already known.[4] However, untransformed depth profiles only provide relative information on the position of features. Since in most experimental systems the locations of interfaces is not known, a translation to a depth scale is required to determine their position and size. To translate to a depth scale it is necessary to determine the sputter times at which polymer–polymer and polymer–substrate interfaces are seen. In this study we examined the first derivative of the intensity of the characteristic ion of the underlying layer ($C_4H_5O^+$ for the polystyrene–PMMA interface and Si^+ for the PMMA–silicon interface) to determine interface locations. It was found that identifying the position of the peak in the first derivative near an interface facilitates reproducible identification of interfacial sputter times. The peak maximum of the first derivative identifies the center of the interface and the full width at half maximum (FWHM) the interfacial width. Table 3 shows the sputter time to the polymer–polymer and polymer–substrate interfaces along with the interface widths measured using this method.

Transformation to depth scale

Having defined interfacial positions in sputter time, it is possible to compare methods of converting sputter time to depth. Fig. 2B–D show the results of three different transformations from sputter time to depth of the representative bilayer depth profile shown in Fig. 2A. The expected position of the polystyrene–PMMA and PMMA–silicon interfaces, based on measured film thickness, is marked by vertical lines (mean) and shaded areas (±1 standard deviation). Each of the three transformation methods are discussed below.

Constant sputter rate. Fig. 2B shows the resulting depth profile when a constant sputter rate is assumed. Here a constant sputter rate of 3.23 nm s^{-1}, calculated from the measured overall bilayer thickness and sputter time to polymer–silicon interface, is applied to the representative bilayer depth profile.

Table 3 Identified interface depths and widths from original and transformed bilayer depth profiles. Depth is determined as the position of the maxima of the first derivative of the characteristic peak of the underlying layer. Width is the FWHM local to the maxima

		PS–PMMA		PMMA–Si	
	Transformation	Depth	Width	Depth	Width
Time, s	N/A	45.5	8.8	69.0	7.3
Distance, nm	Constant	147	28.5	223	23.6
	Step	113	31.6	218	17.5
	Linear	113	31.1	218	17.3

Table 4 Relative thicknesses of polystyrene and PMMA layers in bilayer film predicted using three transformation methods, compared to those expected from AFM measurement

		Transformation method			
		Constant	Step	Linear	AFM
Relative layer thickness	Polystyrene	66.0%	50.5%	51.7%	52.1%
	PMMA	34.0%	49.6%	48.3%	47.9%

The shape of the resulting profile is unaltered as sputter time is simply translated linearly to depth. However, where components exhibit different sputter rates this approximation may lead to incorrect concussions regarding layer thickness and interfacial positions. In the transformed profile, three issues are noted: (1) the polystyrene–PMMA interface appears deeper than expected; (2) the polystyrene overlayer appears thicker than expected and the PMMA underlayer thinner than expected; (3) the continuation of the profile after the polymer–silicon interfaces suggests that significant sputtering into the substrate has occurred.

As the measured depth of the polymer–Si interface is used to define the constant sputter rate, this transformation places the PMMA–silicon interface at exactly at the expected interface position of 223 nm. The polystyrene–PMMA interface is predicted to be at 147 nm, 33 nm deeper than the mean measured thickness of the polystyrene film. This difference in the interface position results in significantly different relative layer thicknesses for polystyrene and PMMA than expected. If the expected interface position was not known, and different sputter rates not considered, this incorrect depth scale could lead to erroneous conclusions as to the thickness of each layer and the locations of the layer interfaces (Table 4).

Sputtering into silicon. It is common for polymer depth profiling studies to be carried out on inorganic substrates such as silicon, indium, titanium or gold. It is known that the sputter rate of inorganic materials is orders of magnitude lower than that of organic materials when using argon clusters.[26] When depth profiles are calibrated using a single depth-time measurement this can lead to the appearance of continued sputtering into the substrate. In Fig. 2B we see that in this reconstruction yields a high Si^+ signal intensity at apparent depths ~100 nm beyond the polymer–substrate interface. While it can be understood that this represents continued sampling of the silicon surface by the analysis beam with little surface sputtering, and may not affect conclusions about a bulk overlayer, it nevertheless is an inaccurate representation of the data. Such substrate erosion artifacts are apparent in a number of studies using simple depth-time transformations. These include depth profiles of HeLa Cells on silicon[30,31] and amino acid multi layers.[6,32] In such cases an untransformed axis of sputter time, ion dose or fluency may be more appropriate if the data set cannot effectively translated to length units.

Step change between component sputter rates. In the second transformation (Fig. 2C) we identify each layer and

assign the sputter rate determined by sputtering through single polymer films. The silicon substrate was assigned a sputter rate of 0.03 nm s^{-1}. For this transformation we switch rates between component bulk sputter rates instantaneously at the time point identified as the center of the interface (see Table 3). This results in several improvements over the constant sputter rate applied previously: (1) significantly closer agreement between the predicted and expected positions of the polymer–polymer and polymer–substrate interfaces; (2) predicted layer thicknesses which are more closely aligned with those expected; and (3) no apparent sputtering into the silicon.

With a step-change between sputter rates in each layer of the film, the predicted polystyrene–PMMA interface position of 113 nm is more closely in line with the expected polystyrene overlayer film thickness of 114 ± 7 nm. The predicted depth of the PMMA–silicon interface (218 nm) is within one standard deviation of the expected overall bilayer film thickness (223 ± 9 nm). This results in apparent layer thicknesses closer to that expected from the measured film thicknesses, and a more accurate profile.

Sputter rate transition across the interface. Since it is unlikely that the interface between the two polymers is absolute, we explored modeling the transition between the two polymers. This should take into account the fact that the transition between two materials often shows a rise and fall of characteristic signals as the sputtering crosses the interface *versus* a sharp step function. The width of, and sputtering behavior within, this region may be factors of (1) interfacial mixing during sample preparation caused by phase separation or lateral variance in interface position; (2) atomic mixing induced by ion beam damage and surface roughening during sputter or analysis cycles; (3) differences in component ionization efficiency. Each of these parameters may interact with one another.

We hypothesized that the depth profile transformation may be further improved by interpolating the transition rate across interfaces. While others have accounted for this region using the relative intensity of characteristic ions for each layer,[16] sputtering behavior may not follow relative ion intensity. To assess how the sputter rate transition across the polymer–polymer interface should be modeled, spun cast films of polystyrene–PMMA blends were prepared from toluene. Quantification of XPS spectra of blended polymer films (Fig. 3A) shows a linear decrease in the intensity of the C1s peak (285 eV), and π–π* shakeup peak (290 eV), and linear increase of the C═O and O1s peaks, as PMMA content is increased in polystyrene–PMMA blends, indicating that blends were well mixed. Film thicknesses of blended polymer films were measured by AFM profiling of scalpel-cut trenches. Films were depth profiled as described for single component films, and sputter rates determined relative to pure polystyrene (Fig. 3B). With increasing polystyrene content an approximately linear decreasing trend in relative sputter rate is observed. Therefore, to further improve the model, we allow the sputter rate to change linearly between known single component sputter rates across the

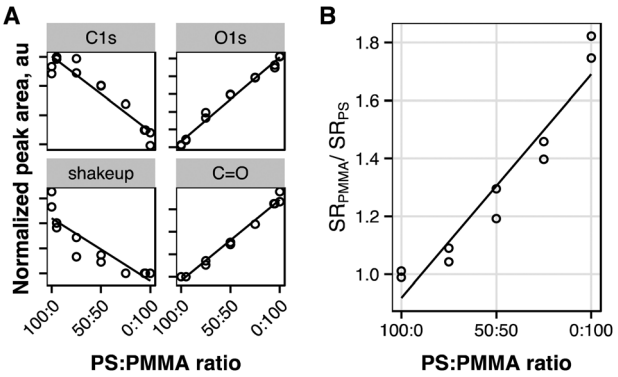

Fig. 3 Characterization of polystyrene–PMMA blend films. (A) XPS peak intensities for blends. (B) Sputter rates of blends relative to pure polystyrene. Linear trend lines shown.

interfacial width. In other systems it may be more appropriate to apply another function to model sputter rate transition: Power-law, exponential or other functions may all be easily applied. These may be applicable where a component with low sputter rate as a single component exhibits a greatly enhanced sputtering in the presence of another component. These effects have been observed in the sputter characteristics of some drug doped polymer materials. For example, Mahoney *et al.* (2005) noted that pluronic-P104 sputtered much more efficiently as a triblock copolymer with PLLA than as a single component material.[33]

Component sputter rates with linear transition. Fig. 2D shows the application of a linear transition between component sputter rates across the width of the interfaces. Pure component sputter rates are still used throughout each layer. The predicted depth of the polystyrene–PMMA interface (113 nm) is seen to be comparable with that predicted using a step change in sputter rates (113 nm). The linear transition between sputter rates softens the shape of the interface, while moving data points slightly deeper (<1 nm) than seen with the sharp transition. Here only a three data points lie in the interfacial region, limiting the capability to alter profile shape during reconstruction. Reconstruction of sputtering phenomena across the polymer–polymer interface would be enhanced by a higher number of data points in interfacial regions.

The PMMA–Si interface appears at 218 nm, in line with that predicted by the step-change transformation, and within one standard deviation of the expected overall bilayer film thickness (223 ± 9 nm). Fig. 4 shows the polymer–Si interfacial region of reconstructed depth profiles in more detail. In the step-change reconstruction peak intensities are seen to abruptly change at the interface. Modeling a linear transition in sputter rate yields a smoother shape to the interface, and more closely reflects the expected differences in sputter rate and component mixing between each sputter-roughened analysis slice within the interfacial region.[34]

Consideration of phase-separation in PS–PMMA blends. Recognizing that polystyrene and PMMA are immiscible and

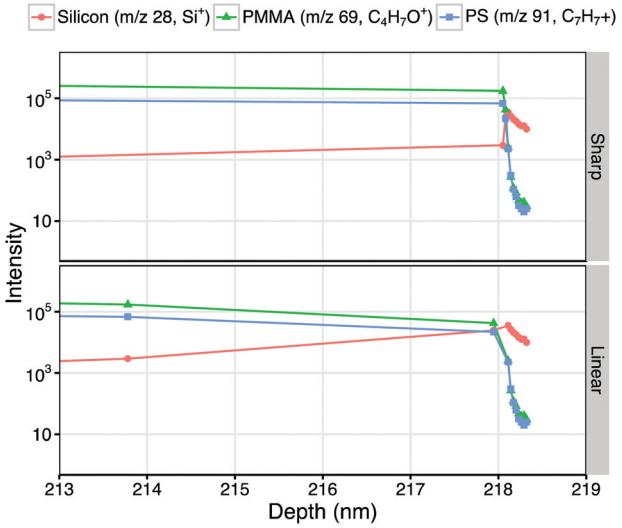

Fig. 4 Enlargements from Fig. 2, showing the polymer–Si interface regions of representative depth profiles reconstructed with sharp (top) and linear (bottom) sputter rate transitions. Intensities of characteristic peaks of each component (silicon: Si^+, *m/z* 28; PMMA: $C_4H_5O^+$, *m/z* 69; polystyrene: $C_7H_7^+$, *m/z* 91) are plotted on a $\log_{10}$ intensity scale against depth from surface.

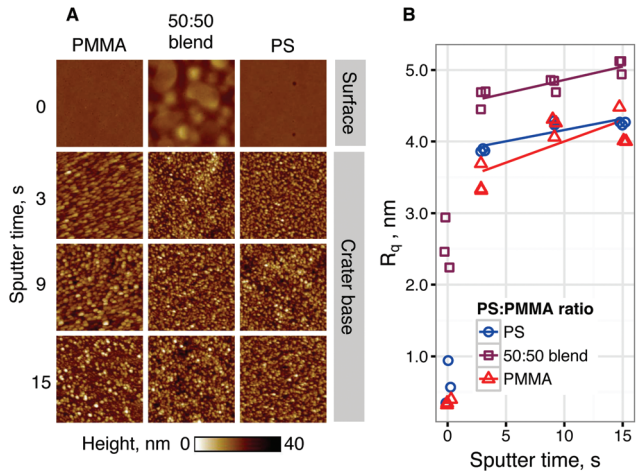

Fig. 5 (A) Representative AFM height maps of PS, PMMA and blended films and crater bases after sputtering for 0 (surface), 3, 9, or 15 (crater bottom) seconds. Images show 1 × 1 μm area. (B) Roughness parameter (R_q) of film surface and sputter crater bases in PS, PMMA and blended films. Linear trend fitted for 5–15 s of sputter time.

may phase-separate, we performed AFM analysis of film surfaces and sputter craters for pure polymers and a 50 : 50 blend. Fig. 5A shows representative AFM height images of film surfaces before sputtering and crater bases after 3, 9 or 15 seconds of sputtering. Fig. 5B shows the roughness (R_q) of film surfaces and crater bases, calculated from representative AFM images. Horizontal line scans across representative AFM images can be found in the ESI.† At the film surface, the blended film exhibits raised domains ~250 nm across and ~10 nm high, indicative of phase separation-induced topography. While phase separation was not promoted by an annealing step, these features are of comparable scale to those previously described for polystyrene–PMMA systems,[35,36] although they may not directly correspond to chemical phase-separations.[37] Such features are not seen at the surface of either pure film, which appear flat (R_q < 1 nm) and uniform.

For all films, the roughness of crater base was substantially higher than for the film surface. Roughness was seen to increase with sputter time. It was seen that the roughness of blended films was significantly higher than for pure films at all sputter times. It was noted that the lateral feature size of the topography after sputtering was smaller than the phase-separated domains seen at the film surface for the 50/50 blend. These results suggest that surface features caused by polymer phase separation are quickly removed by sputter-induced roughening of short lateral feature size and ~10 nm depth range. The phase separation seen here is not expected to adversely influence ToF-SIMS data interpretation, particularly given a ~25-fold difference between the roughness length-scale of crater bases and the SIMS analysis area. No significant difference in polymer–Si interface width was observed for depth profiles of blended polymers.

Errors in depth profile reconstruction introduced by variability in sputter rate determination. Reconstructing a depth profile that is accurate and representative requires confidence in the parameters used to transform the data set, in this case the component sputter rates. Errors in component sputter rates most likely arise from errors in measuring film thicknesses and the sputter time/dose to the polymer–substrate interface since these quantities are used to calibrate the sputter rate. In this study film thickness measurements demonstrated standard deviations of 5–9 nm, approximately 5% of overall film thickness, while the standard deviation for time to polymer–Si interface in polystyrene films was 1.6 seconds (Table 2). The impact of errors in calculated sputter rates can be visualized by reconstructing depth profiles using sputter rates for polystyrene and PMMA randomly sampled from a normal distribution derived from the mean and standard deviation of calculated sputter rates (Fig. 6A). For this figure, the silicon sputter rate was not modified. Significant variation in these profiles can be seen, both in polymer–polymer and polymer–Si interface position, and in relative film thickness. Within each layer, the error in sputter rate determination will linearly correlate with the resulting error in apparent layer thickness. These represent some of the errors that may be introduced to reconstructions through inaccurate sputter rate determination.

In Fig. 6B and C we highlight specific cases of erroneous reconstructions that may arise from the combination of errors in each component sputter rate. When sputter rates are sampled from the same percentile of a normal distribution derived from the mean and standard deviation of calculated sputter rates, errors are introduced both in interface position and layer thickness. Selecting sputter rates from the 5th per-

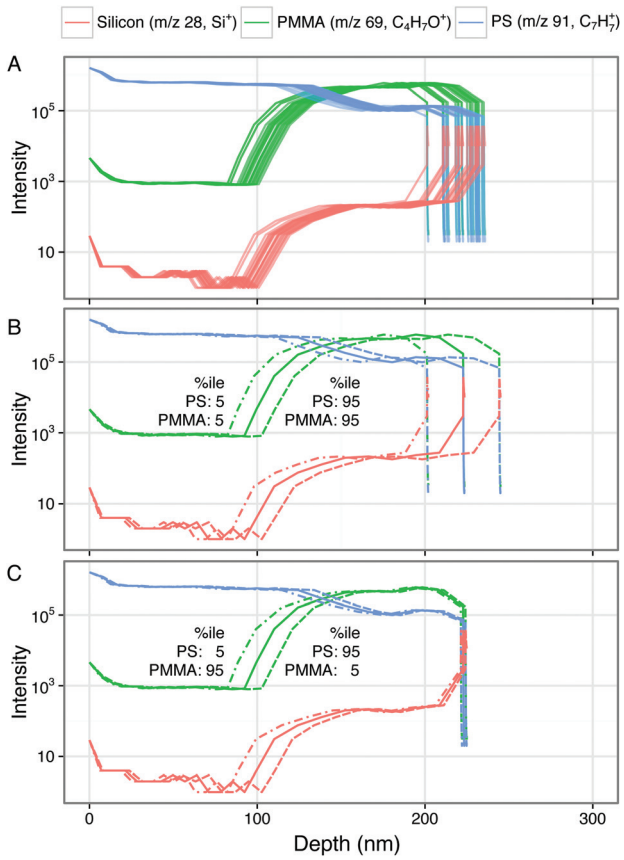

Fig. 6 (A) Depth profiles (n = 20) reconstructed from simulated sputter rates, normally distributed around the mean of the measured sputter rates. (B) Depth profiles reconstructed with sputter rates selected from the 5th (dashed line) or 95th (dot-dashed line) percentile of sputter rates for both polystyrene and PMMA. (C). Depth profiles reconstructed with sputter rates selected from the 5th and 95th percentile (dot-dashed line), or 95th and 5th percentile (dashed line) for polystyrene and PMMA respectively. Profiles reconstructed from mean sputter rates is shown with a solid line.

centile (slower sputter rate than mean) for both polystyrene and PMMA gives apparent polymer–polymer and polymer–Si interfaces shallower than for mean sputter rates (Fig. 6B). When both are selected from the 95th percentile (faster sputter rate than mean) this is reversed, with interface positions deeper than for mean sputter rates. These deviations are ±12 nm for the polymer–polymer interface, and ±22 nm for the polymer–silicon interface. When sputter rates from polystyrene and PMMA samples were selected from percentiles on opposite tails of their respective distribution (5th and 95th, or 95th and 5th), reconstructions place the polymer–Si interface close to that for mean values as the errors in sputter rates cancel one another out (Fig. 6C). However, they continue to displace the apparent polymer–polymer interface position by up to ±12 nm. These scenarios help visualize how errors in the determination of multiple sputter rates mix to produce transformed depth profiles that may not reflect the chemical distribution or thickness of the sample. These results demonstrate the necessity of accurately assigning component sputter rates and validating transformed profiles against expected sample thickness and interface positions. They additionally highlight the potential impact of errors in their determination on reconstructed depth profiles.

Future challenges

Several studies have considered depth profiling and 3D reconstruction of drug-eluting polymer stents.[2,3] In these studies depth scales were assigned using single sputter rates, despite evidence of both drug-polymer phase separation and different sputter rates with drug loading. This represents a scenario where consideration of differences in sputtering may be advantageous. Accurate sputter rate determination is essential for accurate depth profile and 3D reconstruction. In order to account for sputter rate behavior within interfaces, further fundamental studies of blended materials and phase-separated interfaces are required. Different sputter rates may also be expected in biological materials. For sample, mammalian cells have been broadly seen to sputter at the same rate across membrane, cytoplasm and nucleus,[30,38,39] while plant tissues have previously been shown to exhibit different sputter rates between cellular components.[40] Future studies investigating the interface of cells and polymeric scaffolds used for tissue engineering will certainly require consideration of multiple sputter rates.

This study has considered the reconstruction of one-dimensional depth profiles along the z-axis. Correcting for sputter rate differences in 3D ToF-SIMS is a significantly greater challenge. Simple 3D corrections may in the future be accomplished by voxel-stretching, however, an ideal correction would likely need to create new voxels containing reconstructed spectra. Accurate depth profile reconstruction of industrially and clinically relevant, multicomponent, organic and biological systems will require careful and considered application of many factors including correction for sputter rate effects addressed in this study.

Experimental

Preparation of polymer films

10 cm diameter silicon wafers (Silicon Valley Microelectronics, CA) were scored and diced into 1 × 1 cm squares. Silicon squares were cleaned by sequential sonication in ultra-pure, deionized water, dichloromethane, acetone and methanol, with two 15 min washes for each solvent, and allowed to dry before use. Solutions of 30 000 MW polystyrene and 15 000 MW PMMA (both Scientific Polymer Products Inc.), and 25 : 75, 50 : 50 or 75 : 25 mass ratio blends of these, were prepared by dissolving 3% wt : volume of polymer in toluene (PMMA and polystyrene/PMMA blends) or 1-chloropentane (pure polystyrene only) with sonication.

Single component films. Single polymer films of PMMA or polystyrene were prepared by spin coating 120 μl of polymer solution onto cleaned Si wafers at 2200 rpm for 15 seconds.

Excess polymer solution was removed from the edge of the wafer with a laboratory tissue and samples were blown dry with a nitrogen stream. Films of polystyrene–PMMA blends were prepared in the same fashion.

Bilayer films. To prepare bilayer polymer films, first a PMMA film was spun cast from a 3% wt : vol solution in toluene on Si wafer as above. After drying overnight under vacuum to ensure complete solvent evaporation, a polystyrene overlayer was spun cast from a 3% wt : vol solution in 1-chloropenane atop the PMMA film using the same parameters.

Sample storage. Samples were air dried and stored under nitrogen in tissue culture polystyrene multiwell plates for less than 2 weeks until further analysis.

Film thickness measurement

Thickness of polymer films was measured by AFM profiling. Trenches were prepared in polymer films by scoring with the back of a scalpel blade. At least $n = 3$ trenches per film type were profiled using a Dimension Icon-PT AFM (Bruker). The instrument was operated in ScanAsyst mode using ScanAsyst-Air tips (Bruker) with a resonant frequency of 50–90 kHz and a force constant of 0.4 N m^{-1}. Height images were collected across a 90 μm × 90 μm area with scan rate of 0.6 Hz and 256 samples per line. Images were analyzed using NanoScope Analysis v1.5 (Bruker). Representative images ($n = 3$) were flattened using a 1st order algorithm, pre-selecting areas known to represent the film surface. Trench depth was measured using the step measurement tool.

Crater roughness measurement

The roughness of sputter craters produced in spun-cast films of polystyrene, PMMA, or a 50 : 50 blend, was determined by tapping-mode AFM. Craters measuring 600 × 600 μm were produced in polymer films by sputtering using the parameters described for ToF-SIMS data collection below for 3, 9 or 15 seconds. Crater bottoms and original polymer surfaces were analyzed using a Dimension Icon-PT AFM (Bruker). The instrument was operated in tapping mode using Tap300Al-G tips (Budget Sensors) with a resonant frequency of 300 kHz and a force constant of 40 N m^{-1}. Height images were collected across a 1 × 1 μm area with a scan rate of 1 Hz and 256 samples per line. Images were analyzed using NanoScope Analysis v1.5 (Bruker). Representative images ($n = 4$) were flattened using a 1st order algorithm, and roughness (R_q) calculated across the whole image area, excluding any notable artifacts. Horizontal line scans were reconstructed from row 128 of the representative images.

XPS analysis

XPS spectra were obtained from representative bilayer and single-component and blended films ($n = 2$ for each sample) using a Kratos AXIS Ultra DLD (Kratos, Manchester, UK) instrument in the "hybrid" mode (large photoelectron acceptance angle) using a monochromatic Al Kα X-ray source and a nominal photoelectron takeoff angle 0°. Survey scans were collected between 0–1200 eV binding energy for two spots per sample with an 80 eV pass energy and 1 eV step-size. High-resolution scans of the C1s region were acquired with a 20 eV pass energy and 0.1 eV step-size. A low-energy flood gun was used for charge neutralization. XPS data was plotted and analyzed in CasaXPS v2.3 (Casa Software Ltd). All binding energies are referenced to the C1s hydrocarbon peak at 285 eV.

ToF-SIMS data collection

ToF-SIMS depth profiling was performed using an ION-TOF TOF SIMS 5–100 (ION-TOF GmbH, Münster, Germany) instrument equipped with a Bi_n^+ liquid metal ion gun (LMIG) source and an Ar_n^+ gas cluster ion bombardment (GCIB) source. Both sources were arranged with a 45° angle of incidence with respect to the substrate, and rotated 180° around the z-axis with respect to each other. The analysis chamber was maintained at less than 1×10^{-8} mbar. The instrument was operated in a dual-beam, non-interlaced mode with sequential cycles of analysis and sputtering. 25 keV Bi_3^+ clusters were used for analysis and 10 keV Ar_{1000}^+ clusters were used for sputtering. An electron flood gun was used to neutralize charge build-up following sputter and analysis cycles. The target current of the analysis beam was maintained at 0.05 pA. The target current of the sputter source was maintained at 2.5 nA. Positive ion depth profiles were acquired using a dose of 2.9×10^{11} ions per cm^2 per analysis cycle from a 100 × 100 μm area at a 256 × 256 pixel density. Sputtering was carried out for 3 seconds over a 600 × 600 μm area for a dose of 1.3×10^{13} ions per cm^2 per sputter cycle, followed by a 0.5 second pause for charge neutralization. This analysis/sputter cycle was repeated until the intensity of a secondary ion characteristic of the silicon substrate (Si^+) was seen to stabilize, indicating completion of depth profiling through the film. Positive secondary ion spectra were mass calibrated to the CH^+, CH_2^+ and $C_2H_3^+$ peaks. Mass resolution at the $C_2H_3^+$ peak (m/z 27) was typically above 6000. Peaks in the positive ion spectra at m/z 28 (Si^+), 69 ($C_4H_5O^+$) and 91 ($C_7H_7^+$), were identified as characteristic peaks of the Silicon substrate, PMMA, and polystyrene respectively. Depth profile data for these peaks were exported as tab separated files for plotting and transformation to a depth scale in RStudio v0.98 (RStudio Inc).

Determination of interface position

The sputter time to polymer–polymer and polymer–silicon interfaces were determined from the first derivative of the $\log_{10}$ transformed intensity of the characteristic peak of the underlying layer. The location of the maxima nearest the interface position defines the time to the interface. The width of the interface was defined as the full width at half maximum (FWHM) of this peak within the first derivative. If the peak seen in the first derivative is assumed to be Gaussian, which provides a good fit, the boundaries of the FWHM are the time points at which the intensity reaches the commonly used 16% and 84% intensity values used to characterize interfaces.[11] This allows for semi-automated and unbiased interface determination relatively free of subjective operator errors. Both the depth profile and first derivative were fit using LOESS smooth-

ing functions, and intensities predicted in a step-wise fashion using RStudio.

Determining component sputter rates

Component sputter rates for polystyrene and PMMA and polymer blends were calculated using single-component films. Film thicknesses measured by AFM (n = 3) was divided by sputter time to polymer–Si interfaces determined from depth profiles (n = 3). The average sputter rate across bilayer films was determined using the same procedure. While others have observed sputter yields up to 0.01 nm^3 per atom with 10 eV per atom argon clusters,[27] we observed no resulting sputter crater from extensive sputtering of the uncoated silicon substrate. Therefore, we assumed a sputter rate of silicon as 0.03 nm s^{-1} (~0.001 nm^3 per atom at 10 eV per atom), approximately two orders of magnitude lower than that of polystyrene or PMMA, and in line with previously reported sputter rates for silicon with a C_{60} primary ion ranging from 0.01–0.1 nm s^{-1}.[15,41] Molecular dynamic simulations of Ar_n^+ cluster impacts with bare silicon predict similarly low sputter yields at 10 eV per atom.[42]

Depth profile reconstruction

Plotting and depth profile transformation was performed in RStudio. Depth transformations were performed in a step-wise fashion. For step-change and linear transformations interface positions were determined as described above.

Conclusions

Many studies have investigated challenges in sputter depth profiling multicomponent systems using ToF-SIMS including depth resolution, sputter induced damage, and the ability to sputter through a wide range of materials. However, relatively few have addressed correcting for components with different sputter rates through the profile. Using spun-cast bilayer samples of polystyrene and PMMA, this study has shown the following: (1) where the depth profile is transformed to a depth scale using a single constant sputter rate, apparent layer thicknesses do not match expected values, with the predicted polymer–polymer interface shifted ~33 nm deeper than expected (14% of total film thickness). This is due to the fact that the different sputter rates of the components were not accounted for. (2) Accounting for changes in sputter rate with a step-change between known single-component sputter rates provides layer thickness and interface positions in line with measured values. (3) Instantaneous sputter rate transition across an interface is unrealistic, and polystyrene–PMMA blends exhibit a linear increase in sputter rate with increasing PMMA content. (4) Applying a linear transition between component sputter rates across the interface width may yield a profile shape that more closely recapitulates expected sputtering phenomena when sufficient data points are collected across the interfacial width. (5) Accurate determination of sputter rates is critical to producing accurately reconstructed depth profiles. This study provides an easily implemented methodology for the translation of sputter time or ion dose to depth in depth profiles, yielding accurate interface positions and apparent layer thicknesses in scenarios where differences in sputter rates between components may otherwise provide erroneous or misleading results. It is possible that this methodology could be applied to the accurate reconstruction of 3D images of systems exhibiting differences in component sputtering behavior.

Acknowledgements

We gratefully acknowledge support of the research by NIH grant EB-002027 to NESAC/BIO, and thank Gerry Hammer for collection of XPS spectra.

References

1 T. Mouhib, C. Poleunis, N. Wehbe, J. J. Michels, Y. Galagan, L. Houssiau, P. Bertrand and A. Delcorte, *Analyst*, 2013, **138**, 6801–6810.
2 C. M. Mahoney, A. J. Fahey and A. M. Belu, *Anal. Chem.*, 2008, **80**, 624–632.
3 G. L. Fisher, A. M. Belu, C. M. Mahoney, K. Wormuth and N. Sanada, *J. Proteome Res.*, 2009, **81**, 9930–9940.
4 A. G. Shard, R. Havelund, M. P. Seah, S. J. Spencer, I. S. Gilmore, N. Winograd, D. Mao, T. Miyayama, E. Niehuis, D. Rading and R. Moellers, *Anal. Chem.*, 2012, **84**, 7865–7873.
5 J. Bailey, R. Havelund, P. Dubruel, A. G. Shard, I. S. Gilmore, M. R. Alexander and D. J. Scurr, *ACS Appl. Mater. Interfaces*, 2015, **7**, 150106143135007–2659.
6 N. Wehbe, T. Tabarrant, J. Brison, T. Mouhib, A. Delcorte, P. Bertrand, R. Moellers, E. Niehuis and L. Houssiau, *Surf. Interface Anal.*, 2012, **45**, 178–180.
7 C. Bich, R. Havelund, R. Moellers, D. Touboul, F. Kollmer, E. Niehuis, I. S. Gilmore and A. Brunelle, *J. Proteome Res.*, 2013, **85**, 7745–7752.
8 S. Rabbani, A. M. Barber, J. S. Fletcher, N. P. Lockyer and J. C. Vickerman, *J. Proteome Res.*, 2011, **83**, 3793–3800.
9 P. J. Cumpson, J. F. Portoles and N. Sano, *J. Vac. Sci. Technol., A*, 2013, **31**, 020605.
10 P. J. Cumpson, J. F. Portoles, A. J. Barlow and N. Sano, *J. Appl. Phys.*, 2013, **114**, 124313.
11 E.42 Committee, *Standard Guide for Measuring Widths of Interfaces in Sputter Depth Profiling Using SIMS*, ASTM International, West Conshohocken, PA, 2011.
12 S. Hofmann, *Surf. Interface Anal.*, 2003, **35**, 556–563.
13 S. Hofmann, J. Erlewein and A. Zalar, *Thin Solid Films*, 1977, **43**, 275–283.
14 S. Hofmann, *J. Vac. Sci. Technol., A*, 1998, **16**, 1096.
15 A. Wucher, J. Cheng and N. Winograd, *Anal. Chem.*, 2007, **79**, 5529–5539.
16 M. S. Wagner, *Anal. Chem.*, 2004, **76**, 1264–1272.
17 S. Muramoto, J. Brison and D. G. Castner, *Surf. Interface Anal.*, 2010, **43**, 58–61.

18 A. Wucher and H. Oechsner, *Z. Anal. Chem.*, 1989, **333**, 470–473.
19 A. Wucher, J. Cheng and N. Winograd, *Appl. Surf. Sci.*, 2008, **255**, 959–961.
20 A. Wucher and H. Oechsner, *Z. Anal. Chem.*, 1989, **333**, 470–473.
21 W. K. Way, S. W. Rosencrance and N. Winograd, *Surf. Sci.*, 1993, **2**, 67–70.
22 S. W. Rosencrance, W. K. Way and N. Winograd, *Surf. Sci.*, 1993, **2**, 71–75.
23 A. Chilkoti, D. G. Castner and B. D. Ratner, *Appl. Spectrosc.*, 1991, **45**, 209–217.
24 G. P. López, D. G. Castner and B. D. Ratner, *Surf. Interface Anal.*, 1991, **17**, 267–272.
25 D. Ennis, H. Betz and H. Ade, *J. Polym. Sci., Part B: Polym. Phys.*, 2006, **44**, 3234–3244.
26 P. J. Cumpson, J. F. Portoles, A. J. Barlow, N. Sano and M. Birch, *Surf. Interface Anal.*, 2013, **45**, 1859–1868.
27 M. P. Seah, *J. Phys. Chem. C*, 2013, **117**, 12622–12632.
28 V. Cristaudo, C. Poleunis, B. Czerwinski and A. Delcorte, *Surf. Interface Anal.*, 2014, **46**, 79–82.
29 K. Shen, A. Wucher and N. Winograd, *J. Phys. Chem. C*, 2015, **119**, 15316–15324.
30 J. Brison, D. S. W. Benoit, S. Muramoto, M. Robinson, P. S. Stayton and D. G. Castner, *Surf. Interface Anal.*, 2010, **43**, 354–357.
31 J. Brison, M. A. Robinson, D. S. W. Benoit, S. Muramoto, P. S. Stayton and D. G. Castner, *Anal. Chem.*, 2013, **85**, 10869–10877.
32 N. Wehbe, T. Mouhib, A. Delcorte, P. Bertrand, R. Moellers, E. Niehuis and L. Houssiau, *Anal. Bioanal. Chem.*, 2014, **406**, 201–211.
33 C. M. Mahoney, J. Yu and J. A. Gardella, *Anal. Chem.*, 2005, **77**, 3570–3578.
34 D. Mao, A. Wucher and N. Winograd, *Anal. Chem.*, 2009, **82**, 57–60.
35 L. Kailas, J.-N. Audinot, H.-N. Migeon and P. Bertrand, *Appl. Surf. Sci.*, 2004, **231–232**, 289–295.
36 L. Kailas, B. Nysten and P. Bertrand, *Surf. Interface Anal.*, 2004, **36**, 1227–1230.
37 C. Ton-That, A. G. Shard, D. O. H. Teare and R. H. Bradley, *Polymer*, 2001, **42**, 1121–1129.
38 S. Chandra, W. A. Ausserer and G. H. Morrison, *J. Microsc.*, 1987, **148**, 223–229.
39 M. A. Robinson, D. J. Graham and D. G. Castner, *Anal. Chem.*, 2012, **84**, 4880–4885.
40 A. J. Patkin, S. Chandra and G. H. Morrison, *Anal. Chem.*, 1982, **54**, 2507–2510.
41 J. Cheng and N. Winograd, *Anal. Chem.*, 2005, **77**, 3651–3659.
42 N. A. Kubota, D. J. Economou and S. J. Plimpton, *J. Appl. Phys.*, 1998, **83**, 4055–4063.